ACS APPLIED MATERIALS & INTERFACES

Research Article

www.acsami.org

Band Gap Engineering of Boron Nitride by Graphene and Its Application as Positive Electrode Material in Asymmetric Supercapacitor Device

Sanjit Saha,[†,‡] Milan Jana,[†,‡] Partha Khanra,[§] Pranab Samanta,[†,‡] Hyeyoung Koo,[∥] Naresh Chandra Murmu,[†,‡] and Tapas Kuila*[,†]

[†]Surface Engineering & Tribology Division, Council of Scientific and Industrial Research-Central Mechanical Engineering Research Institute, Durgapur 713209, India

[‡]Academy of Scientific and Innovative Research (AcSIR), Anusandhan Bhawan, 2 Rafi Marg, New Delhi 110001, India

[§]Soft Innovative Materials Research Centre, Korea Institute of Science and Technology (KIST), Jeonbuk 565905, South Korea

[∥]Soft Innovative Materials Research Centre, Institute of Advanced Composite Materials, Korea Institute of Science and Technology (KIST), Jeonbuk 565905, South Korea

Supporting Information

ABSTRACT: Nanostructured hexagonal boron nitride (h-BN)/reduced graphene oxide (RGO) composite is prepared by insertion of h-BN into the graphene oxide through hydrothermal reaction. Formation of the super lattice is confirmed by the existence of two separate UV−visible absorption edges corresponding to two different band gaps. The composite materials show enhanced electrical conductivity as compared to the bulk h-BN. A high specific capacitance of ∼824 F g^{-1} is achieved at a current density of 4 A g^{-1} for the composite in three-electrode electrochemical measurement. The potential window of the composite electrode lies in the range from −0.1 to 0.5 V in 6 M aqueous KOH electrolyte. The operating voltage is increased to 1.4 V in asymmetric supercapacitor (ASC) device where the thermally reduced graphene oxide is used as the negative electrode and the h-BN/RGO composite as the positive electrode. The ASC exhibits a specific capacitance of 145.7 F g^{-1} at a current density of 6 A g^{-1} and high energy density of 39.6 W h kg^{-1} corresponding to a large power density of ∼4200 W kg^{-1}. Therefore, a facile hydrothermal route is demonstrated for the first time to utilize h-BN-based composite materials as energy storage electrode materials for supercapacitor applications.

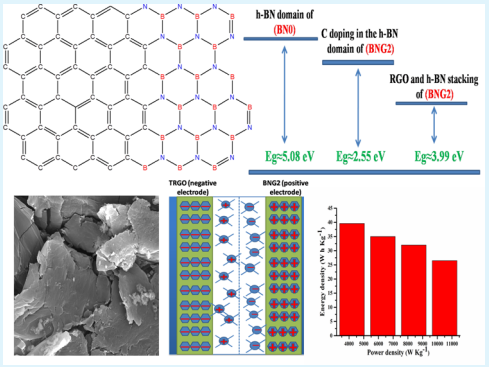

KEYWORDS: *graphene, boron nitride, band gap, supercapacitor, energy density*

1. INTRODUCTION

Constructive and controlled doping can introduce a revolutionary change on the nano materials' properties and at the same time finds application in the fields of photovoltaic and energy storage devices.[1−4] Several types of advanced materials have been explored to investigate their utility in nanoelectronics and energy-harvesting devices.[5−8] Recently developed graphene and its related hybrids also have attracted significant research attention worldwide for various technological and potential applications.[9−13] The hexagonal boron nitride (h-BN) has similar structure to that of graphene where the B and N atoms are substituted by C atoms.[14] However, in comparison to graphene, which has a weak van der Waals force in between the layers, h-BN is connected by strong ionic bonding and has a wide band gap of ∼4−6 eV.[15,16] Pristine h-BN is electrically insulating and does not find applications in the areas of nanoelectronics. Controlled doping can reduce the band gap of h-BN and significantly alter its electrical properties and the resultant hybrid may be regarded as suitable material for nanoelectronics/nanophotonic applications.[16] The bond length in B−N is ∼1.7% higher than that in C−C and, thus, a minimal internal stress is expected upon the interrogation of graphene into the h-BN. Therefore, graphene and h-BN can be selected for perfect alloying.[17] The small difference in electronegativities of B and C atoms is also helpful for the formation of polar covalent bond (BxC) in h-BN/graphene composite as demonstrated by Gao et al.[7] Moreover, the presence of two different chemical species (B and N) in the sublattices of h-BN and the existence of inversion symmetry in the graphene backbone may result in the formation of electrochemically active h-BN/graphene composite.[17] The electrochemical properties of the h-BN/graphene composite are also dependent on the morphological features of h-BN.[18] In addition, the h-BN domains of the h-BN/graphene composite consist of a very

Received: February 25, 2015
Accepted: June 12, 2015
Published: June 12, 2015

DOI: 10.1021/acsami.5b03562
ACS Appl. Mater. Interfaces 2015, 7, 14211−14222

large band gap producing an infinite barrier and the composite network acts like the graphene nanohole superlattice. As a result, small band gaps are generated and the quantum confinement can be noticed at the interface of h-BN and graphene.[19] Ci et al. have shown that the super lattice formation is also possible with hybridized atomic layers of h-BN and graphene nanodomains and the composite acts as low band gap semiconductor.[19] Chang et al. have demonstrated that hybrid h-BN and graphene domains have the small band gap semiconducting property as well as very high electrical conductivity compared to pristine h-BN.[20]

Pristine h-BN has various applications in high-temperature equipment and as a substrate in nanotechnology.[21] However, its electrically insulating property limits its application as electronic materials and in electrochemistry. The opening of a band gap can modify the properties of h-BN suitable for different electronic applications. The remarkable electrical properties of graphene make it appropriate to tune the structure of h-BN and its band gap. Kang et al. have shown that the graphene/boron nitride nanosheets can be used as good microwave-absorbing materials.[22] Levendorf et al. have demonstrated that the graphene/h-BN heterostructure is suitable for atomically thin circuitry.[23] The improved electrical conductivity and the hierarchical arrangement of h-BN/graphene composite suggest its utility in energy storage applications. The application of pristine h-BN is restricted within a traditional dielectric capacitor due to its wide band gap as compared to the materials used for supercapacitor applications.[24] The ongoing demand of the advanced energy storage system can provide large energy and power density as well as long cycling life for the growing market of portable electronic devices which creates a huge interest in supercapacitor research. It can generate large power density, but at the same time the low-energy density as compared to the batteries is still a challenging job. The combined effect of the electric double-layer capacitor (EDLC) and pseudocapacitance can increase the specific capacitance as well as discharging time. However, the low working potential (≈1 V) aqueous electrolytes limits the high-energy applications of the supercapacitor.[25] The ionic/organic electrolyte can provide large working potential but the application of ionic/organic electrolyte is restricted as it is highly expensive and highly hygroscopic in nature. In this regard, asymmetric supercapacitor can be the best solution to achieve higher working potential with aqueous electrolyte. In an asymmetric supercapacitor, two operating potential windows can be generated by using two different types of materials for the two electrodes. The aqueous electrolyte may play the role of faradic-/nonfaradic-type charge-transfer reaction between the electrodes, resulting in significant improvement in energy density.[25] Therefore, it is expected that the h-BN/graphene composite can be regarded as an ideal material for supercapacitor applications because of the EDLC contribution of graphene and the inherent pseudocapacitive nature of the heteroatoms of h-BN.

In this work, we have demonstrated a facile hydrothermal method to develop h-BN/reduced graphene oxide (RGO) composite. Boric acid and ammonia were taken as the source of boron (B) and nitrogen (N). The amount of GO was varied to prepare the electrically conductive composites with different composition. The optical and electrical properties were studied to realize the effect of RGO in the composites. Investigations show the successful formation of composite and enhanced electrical conductivity is appropriate for supercapacitor applications. The electrochemical impedance spectroscopy (EIS) analysis was performed to ensure the ability of the composite material for supercapacitor applications. The electrochemical performances were analyzed by cyclic voltammetry (CV) and charge−discharge experiments. The supercapacitor device exhibited high-energy density along with large specific capacitance corresponding to high current and power density, suggesting the utility of the hybrid materials for energy storage applications.

2. EXPERIMENTAL SECTION

2.1. Reagents. Natural graphite flakes were purchased from Sigma-Aldrich. Hydrochloric acid, sulfuric acid, potassium permanganate, hydrogen peroxide, boric acid, ammonia solution, *N*,*N*-dimethylformamide (DMF), and potassium hydroxide were purchased from Merck, Mumbai, India. Conducting carbon black (EC-600JD, purity: >95%) and polyvinylidene fluoride (PVDF) were purchased from Akzo Nobel Amides Co., Ltd. (Kyungpuk, South Korea). Nickel foam was purchased from Shanghai Winfay New Material Co., Ltd. (Shanghai, China).

2.2. Preparation of h-BN/RGO Composites. Graphite oxide was prepared from natural graphite flakes according to the modified Hummers method.[26] The graphene oxide (GO) dispersion [0.1 g of GO in 20 mL of deionized (DI) water] was prepared after 30 min of sonication. Then ∼1.5 g of boric acid was dissolved in 20 mL of DI water followed by the addition of 20 mL of ammonia solution and sonicated for 10 min. Then the mixed solution was taken into a Teflon-lined autoclave and kept at 150 °C for 2 h. The product was collected by vacuum filtration and dried in a vacuum oven at 50 °C. The sample was named as BNG1. Another two samples were prepared by increasing the amount of GO. About 0.15 and 0.2 g of GO was taken for BNG2 and BNG3, respectively, keeping other parameters constant. Pure boron nitride (BN0) was also prepared following the same methods without adding GO. Hydrothermally reduced GO (HRGO) was prepared under hydrothermal condition (150 °C for 2 h) for structural comparison with the composites. Thermally reduced graphene oxide (TRGO) was prepared through the thermal reduction of GO (∼100 mg) at 500 °C for ∼15 min (under Ar gas atmosphere) and the product was collected for use as negative electrode material in asymmetric supercapacitor device.

2.3. Characterization. X-ray diffraction (XRD) studies of the composite were carried out at room temperature on a D/Max 2500 V/PC (Rigaku Corporation, Tokyo, Japan) at a scan rate of 1° min^{-1} (Cu Kα radiation, λ = 0.15418 nm). Fourier transform infrared (FT-IR) spectroscopy was recorded with a Spectrum 100 FT-IR, PerkinElmer. X-ray photoelectron spectroscopy (XPS) was carried out by using a Kα X-ray photoelectron spectrometer, Thermal Scientific TM. Raman spectra were recorded with Horiba Jobin Yvon (Kyoto, Japan). Field emission scanning electron microscopy (FE-SEM) images were recorded with a Sigma HD (Carl Zeiss, Jena, Germany). Transmission electron microscopy (TEM) images were recorded using JEOL JEM-2100 FS. For sample preparation, the composite sample was dispersed in an ethanol−water mixture (0.1 mg mL^{-1}) by 20 min of ultrasonication followed by drop casting onto a fresh lacey carbon copper grid. Raman spectra of the samples were recorded with a Nanofinder 30 (Tokyo Instruments Co., Osaka, Japan) using a laser wavelength of 514 nm and spot size of 100 mm. The UV−vis spectroscopy was measured by an Agilent Cary 60

DOI: 10.1021/acsami.5b03562
ACS Appl. Mater. Interfaces 2015, 7, 14211−14222

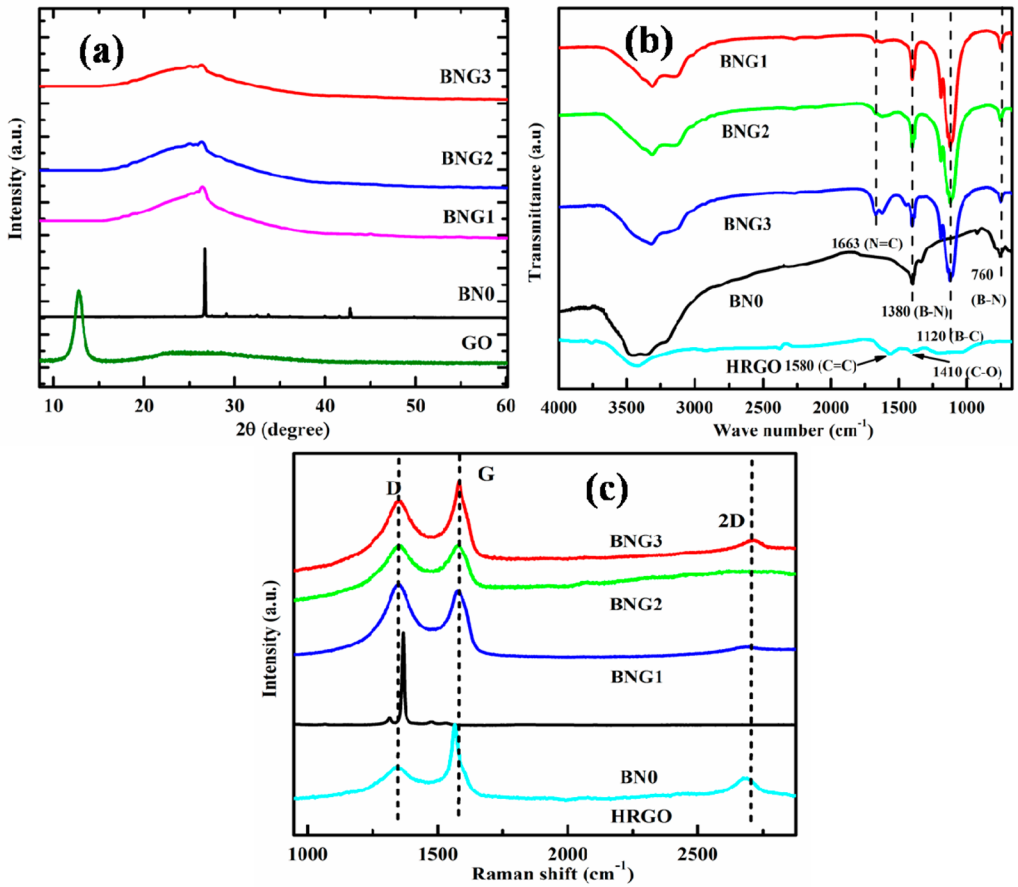

Figure 1. (a) XRD patterns of BN0 and BNG composites. (b) FT-IR spectra of HRGO, BN0, and BNG composites. (c) Raman spectra of HRGO, BN0, and BNG composites.

spectrophotometer. The electrical conductivity was measured using a four-probe set-up with a KEITHLEY delta system consisting of an alternating current and direct current source (model: 6221) and a Nanovoltmeter (model: 2182A). An atomic force microscopy (AFM) image was taken by NX10 Atomic Force Microscope, Park System. Thermogravimetric analysis (TGA) was carried out with a Q50 TGA (TA Instruments, New Castle, DE) in a nitrogen atmosphere with a heating rate of 5 °C min^{-1}.

2.4. Electrochemical Measurements. Electrochemical measurements were carried out with a PARSTAT 4000 (Princeton Applied Research, Oak Ridge, TN) in both three- and two-electrode configurations. The potentiostatic CV, galvanostatic charge−discharge (CD), and EIS were carried out in 6 M aqueous KOH electrolyte. The supercapacitor electrodes were prepared using the composites of ∼80 wt % active materials, 10 wt % PVDF, and 10 wt % carbon black, dispersed in 10 mL of DMF. The electrochemical tests of the individual electrode were carried out in a three-electrode cell, where platinum wire and Ag/AgCl acted as the counter and reference electrodes, respectively. A cleaned Ni foam substrate (5 cm × 0.2 cm) was used as the working electrode and the above said composite was deposited (∼200 mg) on it (area of 1 cm × 0.2 cm). The working electrode was dried inside a vacuum oven at 60 °C for ∼24 h. For asymmetric supercapacitor (ASCs), two pieces of nickel foam (1 cm diameter) were taken and about 15 drops (equivalent to 160 mg) of the above-mentioned composite solution were drop-casted onto the positive electrode. Similarly, the negative electrode material was prepared by mixing 80 wt % TRGO, 10 wt % PVDF, and 10 wt % carbon black, dispersed in 10 mL of DMF. About 25 drops (equivalent to 340 mg) of this composite were casted on the negative electrode. The electrodes were dried under vacuum for 24 h at 60 °C. The two electrodes were placed inside a split test cell (EQ-STC, MTI Corporation, Richmond, CA) to design the ASC. The electrodes were separated by Whatman 42 filter paper impregnated with 6 M aqueous KOH.

3. RESULTS AND DISCUSSION

3.1. Structural and Morphological Analysis. The XRD pattern of BN0 (Figure 1a) shows a sharp peak at 26.7° related to the (002) plane of h-BN.[22,27] The broadening of peak can be observed in the BNG composites. The (002) reflection peak of graphite is shifted to 12.2° in the GO due to the intercalation of oxygen functional groups in its interlayer spacings.[26] The GO is reduced during the formation of BNG composite through hydrothermal reaction and the peak of RGO appears almost at the same position (around 2θ = 23.5°−26.34°) as that of h-BN.[26,27] Therefore, it is very difficult to identify the peaks due to the appearance of a broad band in the range of (2θ = 24°−27°) for the BNG composites. Furthermore, the decrease in particle size and the formation of nanosized domain in the presence of RGO sheets are the main reasons for peak broadening.[22] FT-IR spectroscopy of HRGO, BN0, and the BNG composites are shown in Figure 1b. It shows the appearance of peaks at 760 and 1380 cm^{-1} in the BN0 as well as in the composites. These peaks correspond to the in-plane

DOI: 10.1021/acsami.5b03562
ACS Appl. Mater. Interfaces 2015, 7, 14211−14222

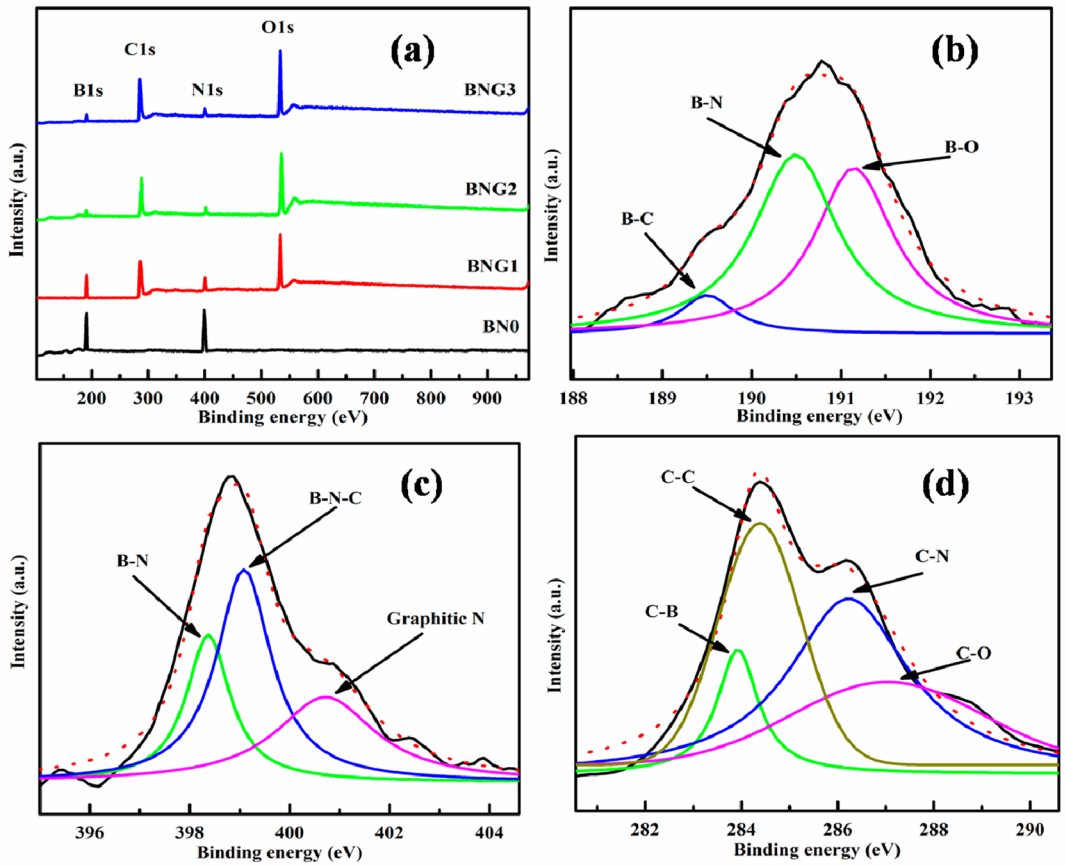

Figure 2. (a) Survey analysis of BN0 and BNG composites. (b) B 1s, (c) N 1s, and (d) C 1s XPS of BNG2.

and out-of-plane bending vibration of B−N.[27,28] The FT-IR spectra of HRGO show sharp peaks at 1580 and1410 cm^{-1} for C═C and C−O bonds, respectively.[29] Almost all of these peaks are absent in the BNG composites. On the other hand, a new peak at 1126 cm^{-1} appeared in the BNGs due to the formation of the B−C bond.[27] The peak at 1670 cm^{-1} indicates the formation of N═C bond in the BNG composites.[30] However, there are no peaks related to N═C and B−C in the BN0. All these observations suggest the formation of hybrid structure for BNG1, BNG2, and BNG3. Figure 1d shows the Raman spectra of HRGO, BN0, and BNG composites. BN0 shows highly intense D band at 1369 cm^{-1} in comparison to the HRGO.[19] The D band appears at 1348 cm^{-1} in the HRGO and composites. The G band indicates the graphite-like structure is not present in the BN0. In contrast, it is present in the HRGO and BNG composites at 1560 and 1578 cm^{-1}, respectively.[19,22] The broadening of the G band indicates lattice distortion and formation of defects in the crystalline structure of the BNG composites.[22] The I_D/I_G ratio obtained from Raman spectra is an indication of degree of disorder and the existence of oxygen-containing functional groups. This I_D/I_G ratio decreases with increasing GO content, indicating improved crystalline nature of the composites.[19] The I_D/I_G ratios are 0.426, 1.06, 0.92, and 0.78 for HRGO, BNG1, BNG2, and BNG3, respectively. In addition, HRGO shows intense 2D band at ∼2700 cm^{-1} and the peak shifts to 2716 cm^{-1} in the composites.

The C 1s spectrum of GO is presented in Figure S1 of the Supporting Information. Three different kinds of oxygen functional groups and the main peak of C 1s (C═C of aromatic rings) can be noticed. The peaks at 285.9, 286.5, and 288.1 eV are assigned to the C−O (epoxy and alkoxy), C═O, and COOH functional groups, respectively.[26] Figure 2a shows the XPS survey of BN0 and BNG composites. The survey spectrum indicates the presence of B, C, N, and O elements in BNG composites while BN0 has only B and N elements. The atomic percentages of O, B, N, and C are determined from the XPS elemental analysis and are summarized in Table 1. It

Table 1. Atomic % of O, C, B, and N of BN0 and BNG Composites Determined from the XPS Elemental Analysis

sample	atomic % of O	atomic % of C	atomic % of B	atomic % of N
BN0			37.22	62.78
BNG1	14.24	35.76	22.36	27.64
BNG2	18.51	43.54	17.49	20.46
BNG3	21.39	47.49	12.78	18.34

shows that the carbon content in the BNG composites increases gradually with GO content. Deconvoluted B 1s peak of BNG2 (Figure 2b) shows the presence of three separate peaks at 189.4, 190.6, and 191.3 eV, respectively. The main peak at 190.6 eV is corresponding to h-BN nanosheet (B−N bonding).[19,22,31] The less intense peak at lower binding energy (189.4 eV) represents the partial formation of B−C bonding in the composite.[19,22,31] The N 1s peak of BNG2 can also be deconvoluted in three separate peaks (Figure 2c). The peaks at 398.2 and 399 eV are due to the presence of h-BN nanosheet (B−N bonding) as well as the presence of B−N−C bonding.[22] Both B 1s and N 1s spectra strongly suggest the formation of separate h-BN domain along with the partial B−C

DOI: 10.1021/acsami.5b03562
ACS Appl. Mater. Interfaces 2015, 7, 14211−14222

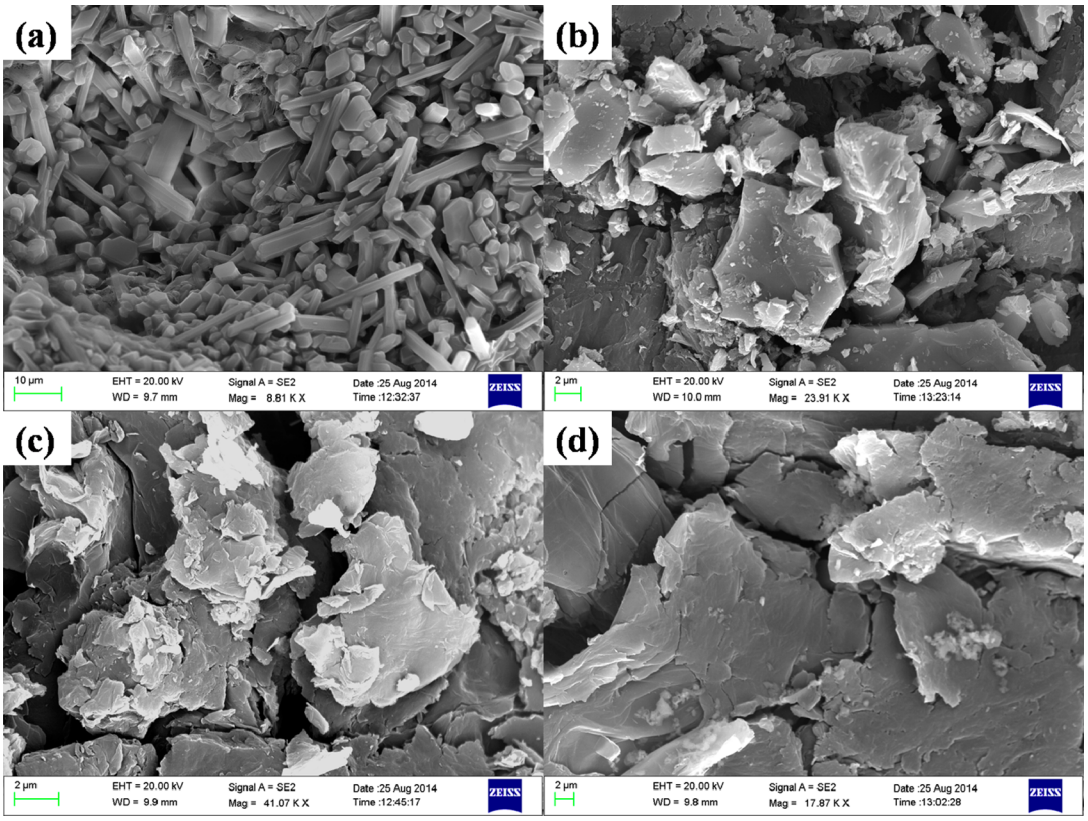

Figure 3. FE-SEM images of (a) BN0, (b) BNG1, (c) BNG2, and (d) BNG3.

and B−N−C bonding in the composite.[19,22] The peak at 400.7 eV in the N 1s spectra may be due to the presence of graphitic N.[22] The C 1s spectrum of BNG2 can be deconvoluted into four separate peaks as shown in Figure 2d. The most intense peak at 284.3 eV ensures the presence of graphitic domains in the composites (C−C bonding).[19,22,31] Relatively small shoulders of B−C (283.9 eV) and C−N (286.2) can also be noticed.[22] Thermal stability of BN0 and BNG composites were studied by TGA and the results are shown in Figure S2 of the Supporting Information. It is seen that the thermal stability of BN0 is very high and the char residue content is ∼98.2% at 700 °C. However, the BNG composites show fast weight loss with increasing temperature. Maximum weight loss can be observed at ∼200 °C for the BNG composites and the char residue contents are 71.0%, 59.9%, and 36.2% for BNG1, BNG2, and BNG3, respectively, at 700 °C. The high weight loss of the composites is attributed to the increased content of GO in the composites.

The FE-SEM image analysis was carried out for the detailed morphological study. Figure 3a shows the formation of large-sized hexagonal rodlike structure of h-BN. The distribution of h-BN particles on the RGO sheets can be seen in the BNG1 (Figure 3b). The sheets become more visible with increasing the amount of GO. The compact stacking of the individual layers of h-BN and RGO is clearly visible in the BNG3 (Figure 3d). TEM image analysis provides a clear view of the hybrid structure. Figure 4a,b represents the TEM and selected area electron diffraction (SAED) pattern images of BNG2. The presence of alternating h-BN and RGO layers is confirmed from the TEM image. The SAED pattern image shows a well-crystalline arrangement of the BNG2. The AFM image of BNG2 is shown in Figure 3c. The lateral size and average thickness were recorded as 39.0 and 3.2 nm, respectively, confirming the formation of a few layers of RGO in the composites. The average thickness is larger than that of the individual layer of graphene sheets which can be ascribed to the alternate stacking of h-BN and RGO sheets in the composites.

3.2. Optical and Electrical Properties. UV−visible absorption spectroscopy was carried out to visualize the electronic property of BN0 and BNG composites as shown in Figure 5a. Band gap was calculated according to the Tauc relationship: $\alpha h\nu = B(h\nu - E_g)^n$, where α is the absorption coefficient, $h\nu$ is the energy of the photon, B is a proportionality constant, E_g represents the optical band gap, and n is the parameter of specific electronic transition within the band due to the light absorption (here, $n = {}^1/_2$).[14,17,22] The extrapolation of the straight portion of the plot of $(\alpha h\nu)^2$ vs $h\nu$ to $\alpha = 0$ determines the band gap (Figure 5b).[19,22,27] GO shows two absorption peaks at 232.6 and 302.3 nm due to $\pi \rightarrow \pi^*$ and n $\rightarrow \pi^*$ transitions, respectively (Figure S3 of the Supporting Information).[26] However, the appearance of a single peak at 284.4 nm in HRGO is related to the resonant excitonic effects of electron−hole interactions in the $\pi \rightarrow \pi^*$ transition (Figure S3 of the Supporting Information). BN0 shows an absorption peak at 220 nm corresponding to the band gap of 5.08 eV.[22,27] However, the composites (BNG1, BNG2, and BNG3) show two separate peaks corresponding to different band gaps as shown in Figure 4a. The change in band gap of h-BN in the composites is due to the different fabrication methods and presence of hexagonal defects. The absorption edge related to the shorter band gap is due to the intermediate structure formed during RGO and h-BN stacking.[19,22,27] The band gaps were calculated as 2.65, 2.55, and 2.42 eV for BNG1, BNG2, and BNG3, respectively (Figure 5b). Interestingly, another

DOI: 10.1021/acsami.5b03562
ACS Appl. Mater. Interfaces 2015, 7, 14211−14222

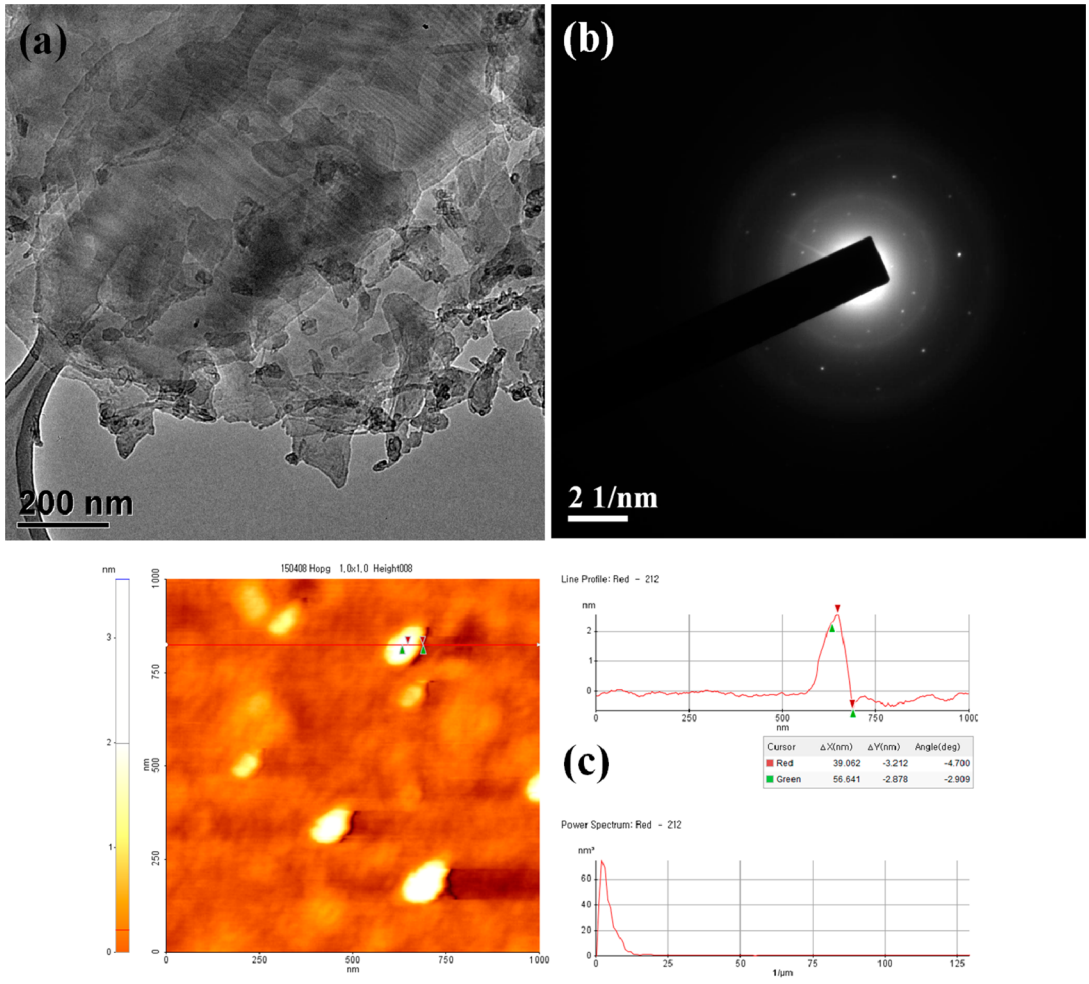

Figure 4. (a) TEM, (b) SAED pattern, and (c) AFM images of BNG2.

absorption peak appeared in the composite at lower wavelength region than that of the RGO but higher with respect to pure h-BN. It may be attributed to the effect of C doping in the h-BN domain of the composites and related to the band gap of the pure h-BN.[19,22,27] The decrease in band gap corresponding to the RGO-doped h-BN domains can be noticed with increasing GO content, suggesting the formation of homogeneous crystalline composite. The measured band gaps are 4.28, 3.99, and 3.96 eV for BNG1, BNG2, and BNG3, respectively (Figure 5b). The formation of the superlattice can also be explained by the appearance of two separate absorbance peaks in the composites as shown in Figure 5a.[19] Furthermore, the formation of hybridized RGO and h-BN atomic layers rather than the substitutionally boron- and nitrogen-doped carbon or alloyed phase can be confirmed by the existence of two separate band gaps.[19] However, it is very difficult to correlate the overall effect of RGO to the BNG composite as the UV−vis absorption is related to the two different domains of the hybrid structure rather than single absorbance peak of graphene edge.[19] The band gap of the hybrid composite can be measured from the linear Arrhenius plot. The electrical conductivity of the powder samples were measured by four-probe technique. The resistivity (ρ) and the electrical conductivity (σ) were measured according to the following relation: $\rho = \pi Rd/(\ln 2)$ and $\sigma = 1/\rho$, where R is the resistance calculated by four-probe method and d is the thickness of the sample under observation.[31,32] BN0 is electrically insulating with electrical conductivity of 2.7 $\times 10^{-5}$ S m^{-1}. The electrical conductivity of GO is also poor due to the presence of oxygen functional groups (52 S m^{-1}). The conductivity increases significantly in RGO (1204 S m^{-1}) due to the restoration of π-electronic conjugated network structure during reduction. Furthermore, the BNG composites show improved electrical conductivity as compared to the BN0 due to the insertion of conducting RGO. The electrical conductivity is recorded as 96, 441, and 545 S m^{-1} for BNG1, BNG2, and BNG3, respectively. Figure 5c shows the variation of electrical conductivity with increasing temperature. The increasing electrical conductivity supports the semiconducting nature of the composites. Furthermore, band gap energy (ΔE_g) can be calculated from the slope of the log ρ vs $10^3/T$ plot and the carrier confinement can be observed within the "graphene paths" embedded in the h-BN domains.[14] Figure 5d shows that the linear fitted data are well-described by $\rho(T) \propto \exp(\Delta E_g/\kappa_B T)$, where κ_B is the Boltzmann constant. The band gaps of BNG1, BNG2, and BNG3 are found to be 61, 14, and 10 meV, respectively.

3.3. Electrochemical Property. Structural and morphological studies confirm the formation of BNG composites. Optical and electrical property analyses ensure the formation of h-BN/RGO hybridized atomic layers which are conducting. However, a material should have low solution resistance with a particular electrolyte for supercapacitor application. EIS measurement in the frequency range of 1−10 kHz with potential amplitude of 10 mV was employed to screen the

DOI: 10.1021/acsami.5b03562
ACS Appl. Mater. Interfaces 2015, 7, 14211−14222

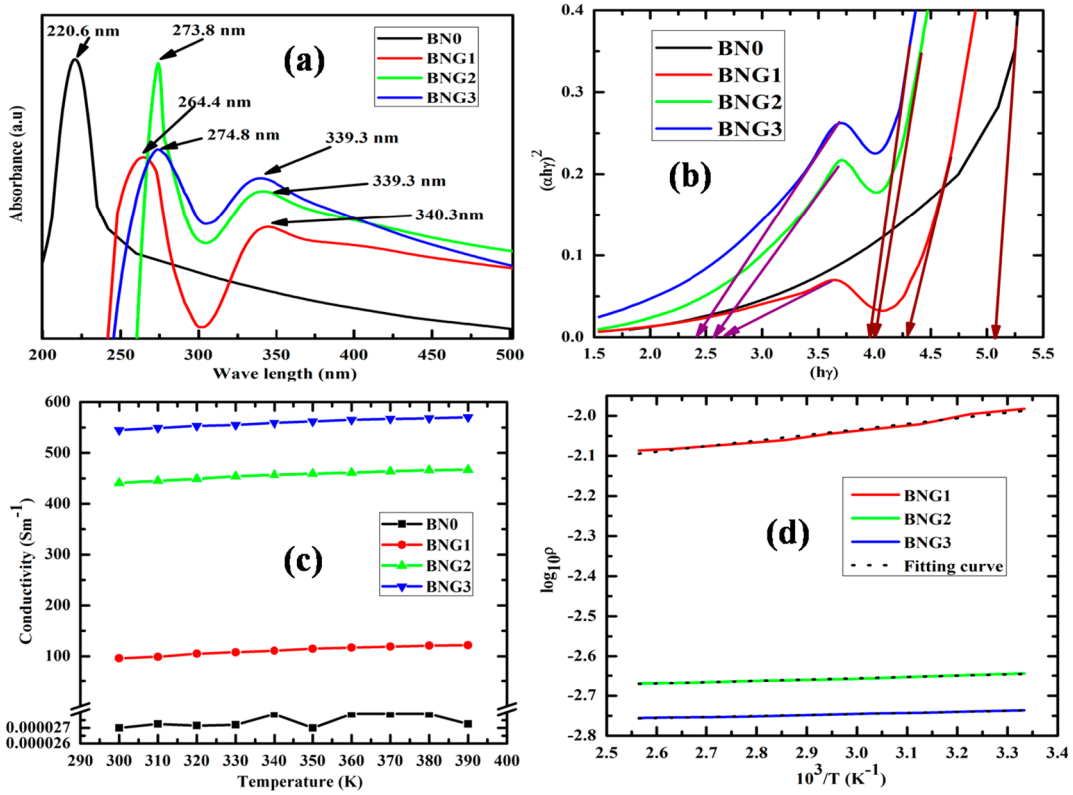

Figure 5. (a) UV−visible absorption spectra, (b) $(\alpha h\nu)^2$ vs $h\nu$ plot, and (c) temperature vs conductivity plot of BN0 and BNG composites. (d) Linear fitted log ρ vs $10^3/T$ plot of BNG composites.

utility of the composites as electrode (three-electrode cell) materials for supercapacitor applications. Figure 6 represents

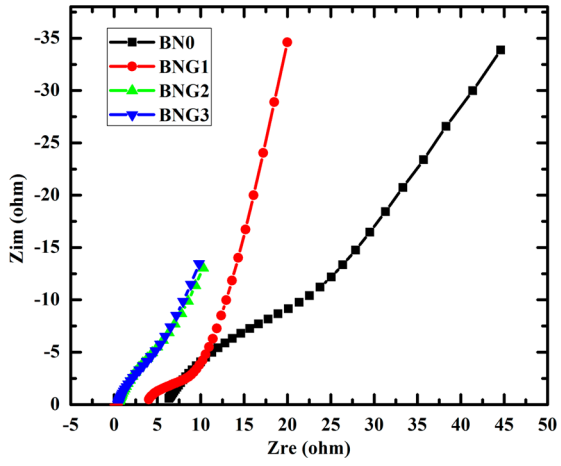

Figure 6. Nyquist plots of BN0 and BNG composites.

the Nyquist plot of pure h-BN and composites. The intersection of the real axis in high-frequency region represents the solution resistance and is related to the charge transfer between the electrode materials and electrolyte.[31,33] It is seen that the BN0 has a high solution resistance of 6.5 Ω, suggesting poor electrochemical performance. The solution resistance decreases to 4.01 Ω in the BNG1 and further decreases in the BNG2 (0.6 Ω) and BNG3 (0.46 Ω), indicating good electrochemical performances. The charge-transfer resistance can be measured from the diameter of the semicircle region corresponding to the real axis and interprets directly to the pseudocapacitive reaction of the electrodes.[31,33] The influence of graphene can be clearly seen as the faradic resistance also decreased from 7.15 to 2.3 Ω for BNG1 as compared to BN0. The charge-transfer resistances are 1.08 and 1.51 Ω for BNG2 and BNG3, respectively. This increase in faradic resistance may be due to the stacking of the RGO sheets and boron layers at high content of GO. The stacking of RGO sheets may prevent the diffusion of ions in solution and affects the charge-transfer resistance.

CV was employed to study the electrochemical behavior of BN0, BNG1, BNG2, and BNG3 in 6 M aqueous KOH electrolyte. The potential window for the electrochemical performance study was selected in the range of −0.1 to 0.4 V (vs AgCl/Ag). Figure 7a represents the comparative study of the CV nature of BN0 and the composites. The prominent oxidation−reduction peaks can be noticed in the BN0. It may be attributed to the fact that the boron and nitrogen atoms are connected by the ionic bond and nitrogen has a different oxidation state. The oxidation state can be altered due to the intercalation with the electrolyte during the redox reaction. It is seen that the width of the CV curve increases with the insertion of GO, maintaining the pseudo nature for all the BNG composites. Deformation in the CV curves can also be observed for BN0 just after increasing the scan rates; however, the composites remain stable even at higher scan rate (Figure S4 of the Supporting Information). Specific capacitance can be calculated from the CV curves using the equation: $C_{CV} = (\int I\, dV)/mV$, where C_{CV} is the specific capacitance (F g^{-1}), I is the response current density (A g^{-2}), V is the potential window, v is the scan rate (mV s^{-1}), and m is the deposited mass on the electrode.[10,34−36] Figure S5a,b of the Supporting Information shows the CV plots and the specific capacitance of GO, HRGO,

DOI: 10.1021/acsami.5b03562
ACS Appl. Mater. Interfaces 2015, 7, 14211−14222

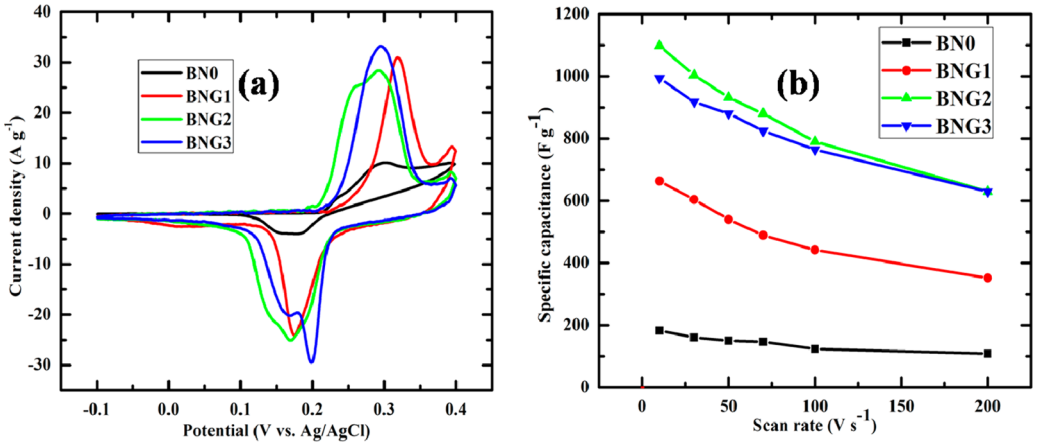

Figure 7. (a) CV plots of BN0 and BNG composites at 10 mV scan rate. (b) Variation of specific capacitance with scan rates for BN0 and BNG composites.

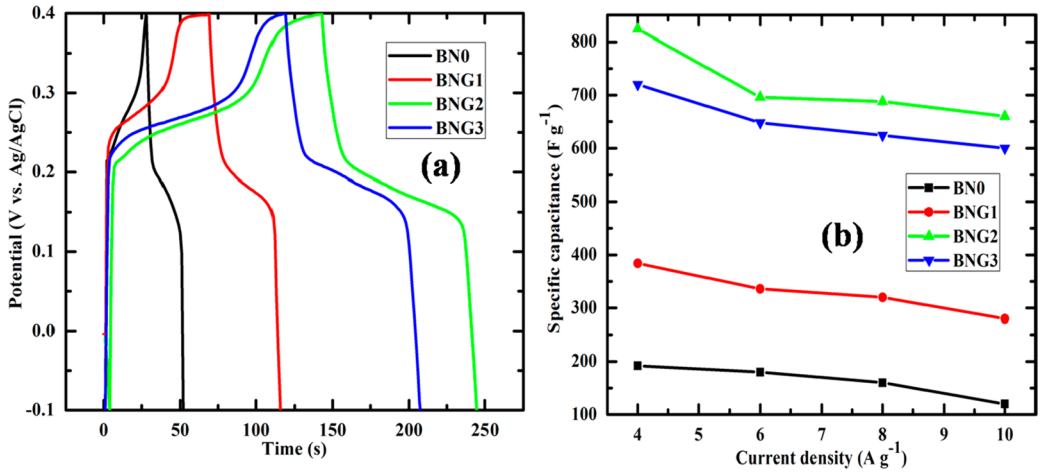

Figure 8. (a) CDs of BN0 and BNG composites at 4 A g^{-1} current densities. (b) Variation of specific capacitance of BN0 and BNG composites at different current densities.

and TRGO at different scan rates. The specific capacitances of GO, HRGO, TRGO, BN0, BNG1, BNG2, and BNG3 are 25, 209, 541, 203, 797, 1098, and 994 F g^{-1} at a scan rate of 10 mV s^{-1}, respectively. Figure 7b represents the variation of specific capacitance of all the samples with increasing scan rates. Stacking of the layers and increase in the faradic resistance may be the reason for the lower specific capacitance of BNG3 as compared to that of BNG2. It has been found that the RGO contributed to the specific capacitance through 0 as well as pseudocapacitance due to the presence of the remaining oxygen functional groups. However, the capacitive nature of RGO is deteriorated due to the stacking of GO sheets during reduction. Pure boron nitride has similar structure to that of the graphite with conjugated double bonds and free π electrons (Figure S6 of the Supporting Information). The insertion of h-BN in the interlayer spaces of RGO acts as spacer molecules and prevents the restacking of GO sheets. Furthermore, the free π electron and the change in the oxidation state of B and N atoms contribute to the additional charge storage capacity of the BNG2 composites. The oxidation state of boron and nitrogen is altered during charging and discharging. The charge storage mechanism in the BNG composites arises from the synergistic effect of RGO and boron nitride. The increase in GO content in the BNG3 causes restacking of RGO sheets and prevents the diffusion of ions in solution affecting the charge-transfer resistance.

Galvanostatic charge−discharge (CD) curves show the appearance of sharp and large IR drop for all the samples (Figure 8a). CD was measured at different current densities starting from 4 to 10 A g^{-1}. The specific capacitance can be calculated in terms of the discharge time according to the equation: $C_{CD} = I\Delta t/mV$, where CD is the specific capacitance (F g^{-1}), I is the discharging current (A g^{-2}), V is the potential window (V), and m is the deposited mass on the electrode.[29,33,34,37] The presence of RGO increases the discharging time effectively. The charging and discharging profiles of all the samples with different current densities are presented in Figure S7 of Supporting Information. Figure 8b represents the variation of specific capacitance for all the samples with increasing current density. Pure BN0 exhibits the specific capacitance of 182.8 F g^{-1} at a current density of 4 A g^{-1}. In contrast, the specific capacitances measured at the same current density are 384, 824, and 720 F g^{-1} for BNG1, BNG2, and BNG3, respectively. At very high current density of 10 A g^{-1}, the retention of specific capacitance for BNG1, BNG2, and BNG3 are 72%, 81%, and 83%, respectively, while the retention is only 62% for BN0. The Coulombic efficiency is quite low (below 75%) when the CD is measured from −0.1 to 0.4 V. To improve the Coulombic efficiency, the CD is further examined

DOI: 10.1021/acsami.5b03562
ACS Appl. Mater. Interfaces 2015, 7, 14211−14222

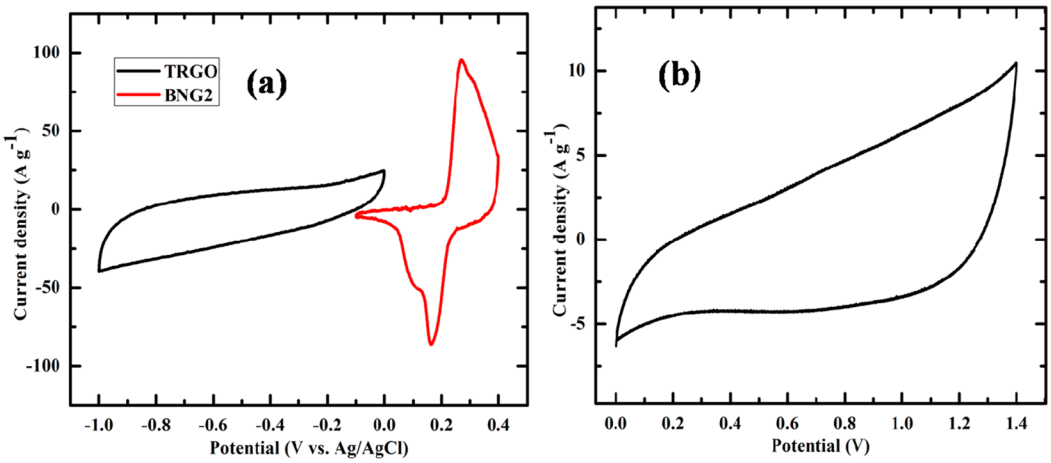

Figure 9. (a) Comparative CV curves of TRGO and BNG2 performed at three-electrode cell. (b) CV of optimized BNG2/TRGO ASC.

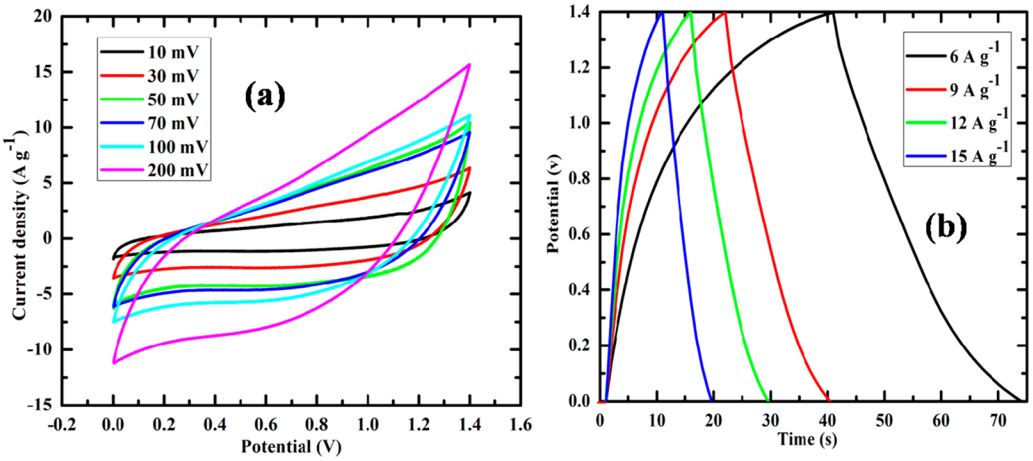

Figure 10. (a) CVs of ASC at different scan rates and (b) CDs of ASC at different current densities.

up to 0.35 V. The calculated specific capacitance are 220.4, 409.8, 897.7, and 773.3 F g^{-1} for BN0, BNG1, BNG2, and BNG3, respectively, and the Coulombic efficiency is more than 90% (Figure S8 of the Supporting Information). Furthermore, the BNG composites show large IR drop with the loss of specific capacitance. To investigate the effective specific capacitance C_{Total} is calculated according to the relation $C_{Total} = I\Delta T_{Total}/mV_{Total}$, where T_{Total} and V_{Total} are the discharging time and potential window measure after the IR drop (0.23 V). The value of the C_{Total} of BN0 and BNG composite with different current density is submitted in the Table S1 of the Supporting Information.

3.4. Electrochemical Characterization of Asymmetric Supercapacitor. The composite materials show high specific capacitance but suffer from the low potential window and large IR drop. CV curves obtained from the three-electrode measurement show that the materials can be used as the positive electrode. Asymmetric supercapacitor can be made with another material that can act as the negative electrode. TRGO has the potential range of 0 to −1 V and exhibits good EDLC character (Figure 9a). Both the positive and negative electrode materials were deposited on the nickel foam. For the asymmetric configuration, the mass balance was done according to the following relation: $(m_+/m_-) = (C_- \times \Delta E_-/C_+ \times \Delta E_+)$, where m_+ and m_- are the mass of the positive and negative electrodes, C_+ and ΔE_+ are the specific capacitance and potential window (calculated from the three-electrode measurement) for positive electrode, and C_ and ΔE_- are the specific capacitance and potential window of the negative electrode measured at the same scan rate.[10,23,38,39] The mass ratio for BNG2 and TRGO was optimized as m_{BNG2}/m_{RGO} = 0.68 in the ASC cell.

The ASC shows a large potential window of 1.4 V (Figure 9b). Figure 10a shows the CV plot of ASC at various scanning rates and Figure 10b represents the CD plot at different current densities. The peak current increases progressively with increasing scan rate of CV and the curves are almost symmetric even at the higher scan rate with good current response. The IR drop is minimized as compared to the three-electrode results and exhibit full contribution of the specific capacitance in the studied range.

The specific capacitance is found to be 145.7 F g^{-1} at a current density of 6 A g^{-1} and about 66% of retention in specific capacitance is recorded even at a very high current density of 15 A g^{-1} (Figure 11a). The C_{Total} and the corresponding energy and power density of the ASC at different current densities are given in Table S2 of the Supporting Information. Figure 11b shows the retention of specific capacitance charged at 1.4 V as a function of cycle number. The increase in specific capacitance after 600 cycles may be due to the surface wetting during extended cycling. Further increase in the available active sites during the initial

DOI: 10.1021/acsami.5b03562
ACS Appl. Mater. Interfaces 2015, 7, 14211−14222

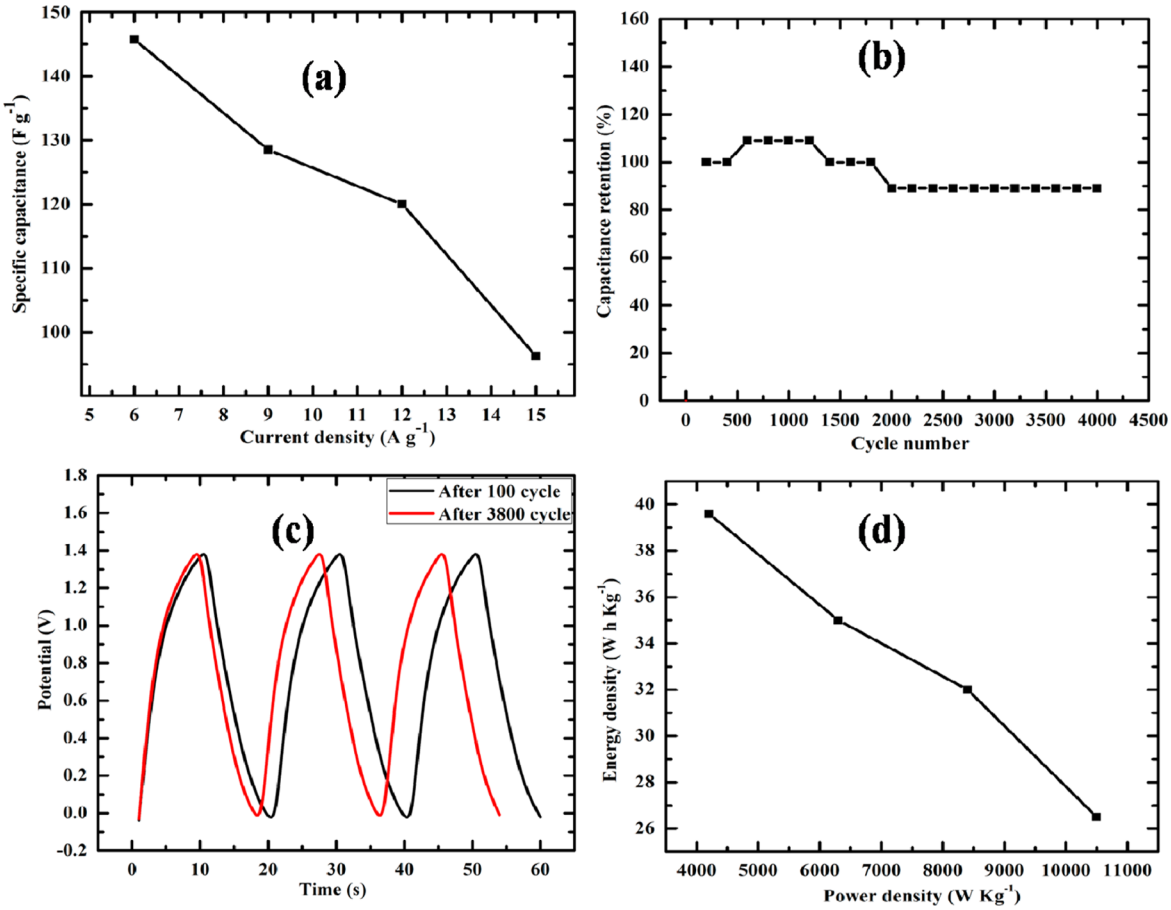

Figure 11. (a) Variation of specific capacitance of ASC with current densities, (b) cycling performance of ASC at a current density of 15 A g^{-1}, (c) CD curves of ASC at a current density of 15 A g^{-1} after different extended periods of cycling, and (d) Ragone plot of ASC.

cycling process may enhance the supercapacitor performances. The ASC displays an excellent long cycle life of only 89% retention even after 4000 cycles. Figure 11c represents the comparative CD plot (at a current density 15 A g^{-1}) of ASC after 100 and 3800 cycles, respectively. The undistorted nature of the CD after 3800 cycles ensured the stability of the ASC. The energy density (E_D) and power density (P_D) of the ASC can be calculated according to the following relations: $E_D = CV^2/2$ and $P_D = E_D/\Delta T$, where C is the specific capacitance calculated from the CD, V is the potential window, and the ΔT is the discharging time calculated from the CD.[39−41] A high-energy density of 39.6 W h kg^{-1} was achieved at a power density of 4200 W kg^{-1} (Figure 11d). Figure 12 represents the Nyquist plot of the ASC cell. The measured solution and faradaic resistances are 1.2 and 1.7 Ω, respectively. The low solution resistance suggests that the ASC cell can be assembled in series for high voltage application with minimum loss of energy. Table S3 of the Supporting Information shows the promising properties of ASC as compared to those of the recently reported graphene-based electrode materials. The comparison of the capacitive performance of the BNG composites and the ASC with other B- and N-based materials are shown in Table S4 of the Supporting Information. It is seen that the capacitive performances of the boron nitride-based composites are superior as compared to those of similar types of materials. Even at a very high power density of 10 500 W h kg^{-1}, the current density still remains at 26.15 W kg^{-1}, which is

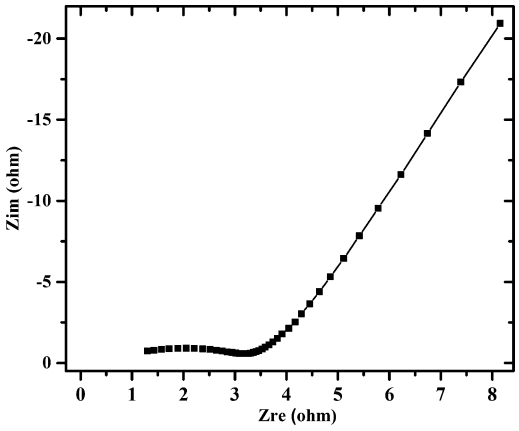

Figure 12. Nyquist plot of ASC.

encouraging for the implementation of BNG-based materials in supercapacitor devices.

4. CONCLUSIONS

A facile and single-step hydrothermal method was described to prepare a h-BN/RGO hybrid nanostructure. The band gap of the insulator h-BN was successfully reduced by increasing the amount of GO content in the composite. The hybridized atomic layer of RGO and h-BN exhibited two separate UV absorption peaks, signifying the existence of two different domains in the composites. The presence of RGO increased

DOI: 10.1021/acsami.5b03562
ACS Appl. Mater. Interfaces 2015, 7, 14211−14222

the electrical conductivity of h-BN and provided good ion exchange with the electrolyte by decreasing the solution resistance as well as the charge-transfer resistance. The super lattice microstructure exhibited a prominent pseudo nature incorporated with EDLC. The precise amount of RGO content in the h-BN provided high specific capacitance of ~824 F g^{-1}. A large potential window was also achieved by constructing ASC with BNG2 as the positive electrode and TRGO as the negative electrode. The specific capacitance of the ASC cell was 145.7 F g^{-1} at a current density of 6 A g^{-1} and the almost zero IR drop suggests that the selected potential window is perfect for the electrode materials. The maximum energy density of 39.6 W h kg^{-1} was achieved corresponding to the power density of 4200 W kg^{-1} and the Ragone plot ensured the utility of ASC even at very high power density of 10 500 W kg^{-1}. The cell maintains invariant electrochemical performance at a high current density of 15 A g^{-1}. The ASC showed long life stability and undistorted nature of CD even after 4000 cycles. These intriguing performances of ASC suggest the utility of boron nitride-based composite for energy storage applications.

■ ASSOCIATED CONTENT

Ⓢ Supporting Information

UV−visible absorption spectra of GO and HRGO, CVs of BN0, BNG1, BNG2, and BNG3 at different scan rates, TGA analysis of CDs of BN0, BNG1, BNG2, and BNG3, CVs of GO, HRGO, and TRGO at 10 mV s^{-1} scan rate, atomic structure of h-BN, and CD plot of BN0 and BNG composites from −0.1 to 0.35 V. BN0, BNG1, BNG2, and BNG3 at different current densities, table of the variation of C_{total} of BN0 and BNG composites with different current densities, table of the variation of C_{total}, energy and power densities of ASC with different current densities of BN0 and BNG composites with different current densities, comparison table of the specific capacitance, energy and power densities of different graphene-based asymmetric supercapacitor, and comparison table of the different B- and N-based supercapacitor performances. The Supporting Information is available free of charge on the ACS Publications website at DOI: 10.1021/acsami.5b03562.

■ AUTHOR INFORMATION

Corresponding Author

*Phone: 91-9647205077. Fax: 91-343-2548204. E-mail: tkuila@gmail.com (T.K.).

Notes

The authors declare no competing financial interest.

■ ACKNOWLEDGMENTS

Authors are thankful to the Director of CSIR-CMERI. Authors are also thankful to the Department of Science and Technology, New Delhi, India, for the financial support from the DST-INSPIRE Faculty Scheme - INSPIRE Programme (IFA12CH-47) and Council of Scientific and Industrial Research, New Delhi, India, for funding MEGA Institutional project (ESC0112/RP-II).

■ REFERENCES

(1) Qu, L.; Liu, Y.; Baek, B. J.; Dai, L. Nitrogen-Doped Graphene as Efficient Metal-Free Electrocatalyst for Oxygen Reduction in Fuel Cells. *ACS Nano* **2010**, *4*, 1321−1326.

(2) Lin, T.; Huang, F.; Liang, J.; Wang, Y. A Facile Preparation Route for Boron-Doped Graphene, and Its CdTe Solar Cell Application. *Energy Environ. Sci.* **2011**, *4*, 862−865.

(3) Reddy, M. L. A.; Srivastava, A.; Gowda, R. S.; Gullapalli, H.; Dubey, M.; Ajayan, M. P. Synthesis of Nitrogen-Doped Graphene Films for Lithium Battery Application. *ACS Nano* **2010**, *4*, 6337−6342.

(4) Xiang, C.; Li, M.; Zhia, M.; Manivannan, A.; Wu, N. A Reduced Graphene Oxide/Co_3O_4 Composite for Supercapacitor Electrode. *J. Power Sources* **2013**, *226*, 65−70.

(5) Chen, M. S.; Ramachandran, R.; Mani, V.; Saraswathi, R. Recent Advancements in Electrode Materials for the High Performance Electrochemical Supercapacitors: A Review. *Int. J. Electrochem. Sci.* **2014**, *9*, 4072−4085.

(6) Shown, I.; Ganguly, A.; Chen, L. C.; Chen, K. H. Conducting Polymer-Based Flexible Supercapacitor. *Energy Sci. Eng.* **2015**, *3*, 2−26.

(7) Gao, Z. D.; Zhu, X.; Li, Y.; Hang; Zhou, X.; Song, Y. Y.; Schmuki, P. Carbon Cladded TiO_2 Nanotubes: Fabrication and Use in 3D-RuO_2 Based Supercapacitors. *Chem. Commun.* **2015**, *51*, 7614−7617.

(8) Hu, X.; Zhang, W.; Liu, X.; Mei, Y.; Huang, Y. Nanostructured Mo-Based Electrode Materials for Electrochemical Energy Storage. *Chem. Soc. Rev.* **2015**, *44*, 2376−2404.

(9) Fan, Z.; Zhao, Q.; Li, T.; Yan, J.; Ren, Y.; Feng, J.; Wei, T. Easy Synthesis of Porous Graphene Nanosheets and Their Use in Supercapacitors. *Carbon* **2012**, *50*, 1699−1703.

(10) Yan, J.; Fan, Z.; Sun, W.; Ning, G.; Wei, T.; Zhang, Q.; Zhang, R.; Zhi, L.; Wei, F. Advanced Asymmetric Supercapacitors Based on $Ni(OH)_2$/Graphene and Porous Graphene Electrodes with High Energy Density. *Adv. Funct. Mater.* **2012**, *22*, 2632−2641.

(11) Cao, J.; Wang, Y.; Zhou, Y.; Ouyang, H. J.; Jia, D.; Guo, L. High Voltage Asymmetric Supercapacitor Based on MnO_2 and Graphene Electrodes. *J. Electroanal. Chem.* **2013**, *689*, 201−206.

(12) Wang, C. C.; Chen, C. H.; Lu, Y. S. Manganese Oxide/Graphene Aerogel Composites as an Outstanding Supercapacitor Electrode Material. *Chem.—Eur. J.* **2014**, *20*, 517−523.

(13) Jeong, M. H.; Lee, W. J.; Shin, H. W.; Choi, J. Y.; Shin, J. H.; Kang, K. J.; Choi, W. J. Nitrogen-Doped Graphene for High-Performance Ultracapacitors and the Importance of Nitrogen-Doped Sites at Basal Planes. *Nano Lett.* **2011**, *11*, 2472−2477.

(14) Golberg, D.; Bando, Y.; Huang, Y.; Terao, T.; Mitome, M.; Tang, C.; Zhi, C. Boron Nitride Nanotubes and Nanosheets. *ACS Nano* **2010**, *4*, 2979−2993.

(15) Panchakarla, S. L.; Subrahmanyam, S. K.; Saha, K. S.; Govindaraj, A.; Krishnamurthy, R. H.; Waghmare, V. U.; Rao, R. N. C. Synthesis, Structure, and Properties of Boron- and Nitrogen-Doped Graphene. *Adv. Mater.* **2009**, *21*, 4726−4730.

(16) Xue, Y.; Liu, Q.; He, G.; Xu, K.; Jiang, L.; Hu, X.; Hu, J. Excellent Electrical Conductivity of the Exfoliated and Fluorinated Hexagonal Boron Nitride Nanosheets. *Nanoscale Res. Lett.* **2013**, *8*, 49.

(17) Bhandary, S.; Sanyal, B. Graphene-Boron Nitride Composite: A Material with Advanced Functionalities. In *Composites and Their Properties*, Hu, Ning, Ed.; InTech: Rijeka, Croatia, 2012; http://www.intechopen.com/books/composites-and-their-properties/graphene-boron-nitride-composite-a-material-with-advanced-functionalities, ISBN 978-953-51-0711-8.

(18) Nozaki, H.; Itoh, S. Structural Stability of BC_2N. *J. Phys. Chem. Solids* **1996**, *57*, 41−49.

(19) Ci, L.; Song, L.; Jin, C.; Jariwala, D.; Wu, D.; Li, Y.; Srivastava, A.; Wang, F. Z.; Storr, K.; Balicas, L.; Liu, F.; Ajayan, M. P. Atomic Layers of Hybridized Boron Nitride and Graphene Domains. *Nat. Mater.* **2010**, *9*, 430−435.

(20) Chang, K. C.; Kataria, S.; Kuo, C. C.; Ganguly, A.; Wang, Y. B.; Hwang, Y. J.; Huang, J. K.; Yang, H. W.; Wang, B. S.; Chuang, H. C.; Chen, M.; Huang, I. C.; Pong, F. W.; Song, J. K.; Chang, J. S.; Guo, H. J.; Tai, Y.; Tsujimoto, M.; Isoda, S.; Chen, W. C.; Chen, C. L.; Chen, H. K. Band Gap Engineering of Chemical Vapor Deposited Graphene by In-Situ BN Doping. *ACS Nano* **2013**, *7*, 1333−1341.

(21) Dean, R. C.; Young, F. A.; Meric, I.; Lee, C.; Wang, L.; Sorgenfrei, S.; Watanabe, K.; Taniguchi, T.; Kim, P.; Shepard, L. K.; Hone, J. Boron Nitride Substrates for High-Quality Graphene Electronics. *Nat. Nanotechnol.* **2010**, *5*, 722−726.

(22) Kang, Y.; Chu, Z.; Zhang, D.; Li, G.; Jiang, Z.; Cheng, H.; Li, X. Incorporate Boron and Nitrogen into Graphene To Make BCN

DOI: 10.1021/acsami.5b03562
ACS Appl. Mater. Interfaces 2015, 7, 14211−14222

Hybrid Nanosheets with Enhanced Microwave Absorbing Properties. *Carbon* **2013**, *61*, 200−208.
(23) Levendorf, P. M.; Kim, J. C.; Brown, L.; Huang, Y. P.; Havener, W. R.; Muller, A. D.; Park, J. Graphene and Boron Nitride Lateral Heterostructures for Atomically Thin Circuitry. *Nature* **2012**, *488*, 627−632.
(24) Guo, N.; Wei, J.; Jia, Y.; Sun, H.; Wang, Y.; Zhao, K.; Shi, X.; Zhang, L.; Li, X.; Cao, A.; Zhu, H.; Wang, K.; Wu, D. Fabrication of Large Area Hexagonal Boron Nitride Thin Films for Bendable Capacitors. *Nano Res.* **2013**, *6*, 602−610.
(25) Chang, J.; Jin, M.; Yao, F.; Kim, H. T.; Le, T. V.; Yue, H.; Gunes, F.; Li, B.; Ghosh, A.; Xie, S.; Lee, H. Y. Asymmetric Supercapacitors based on Graphene/MnO_2 Nanospheres and Graphene/MoO_3 Nanosheets with High Energy Density. *Adv. Funct. Mater.* **2013**, *23*, 5074−5083.
(26) Jana, M.; Saha, S.; Khanra, P.; Murmu, C. N.; Srivastava, K. S.; Kuila, T.; Lee, H. J. Bio-Reduction of Graphene Oxide using Drained Water From Soaked Mung Beans (Phaseolus Aureus L.) and Its Application as Energy Storage Electrode Material. *Mater. Sci. Eng., B* **2014**, *186*, 33−40.
(27) Gao, G.; Gao, W.; Cannuccia, E.; Tijerina, T. J.; Balicas, L.; Mathkar, A.; Narayanan, N. T.; Liu, Z.; Gupta, K. B.; Peng, J.; Yin, Y.; Rubio, A.; Ajayan, M. P. Artificially Stacked Atomic Layers: Toward New Van Der Waals Solids. *Nano Lett.* **2012**, *12*, 3518−3525.
(28) Wang, L.; Sun, C.; Xu, L.; Qiana, Y. Convenient Synthesis and Applications of Gram Scale Boron Nitride Nanosheets. *Catal. Sci. Technol.* **2011**, *1*, 1119−1123.
(29) Wang, L.; Ye, Y.; Lu, X.; Wen, Z.; Li, Z.; Hou, H.; Song, Y. Hierarchical Nanocomposites of Polyaniline Nanowire Arrays on Reduced Graphene Oxide Sheets for Supercapacitors. *Sci. Rep.* **2013**, *3*, 3568.
(30) Xue, Y.; Yu, D.; Dai, L.; Wang, R.; Li, D.; Roy, A.; Lu, F.; Chen, H.; Liu, Y.; Qu, J. Three-Dimensional B,N-Doped Graphene Foam as a Metal-Free Catalyst for Oxygen Reduction Reaction. *Phys. Chem. Chem. Phys.* **2013**, *15*, 12220−12226.
(31) Saha, S.; Jana, M.; Samanta, P.; Murmu, C. N.; Kim, H. N.; Kuila, T.; Lee, H. J. Hydrothermal Synthesis of Fe_3O_4/RGO Composites and Investigation of Electrochemical Performances for Energy Storage Applications. *RSC Adv.* **2014**, *4*, 44777−44785.
(32) Dhibar, S.; Bhattacharya, P.; Hatui, G.; Sahoo, S.; Das, K. C. Preparation of CTAB Assisted Hexagonal Platelet $Co(OH)_2$/Graphene Hybrid Composite as Efficient Supercapacitor Electrode Material. *ACS Sustainable Chem. Eng.* **2013**, *1*, 1135−1142.
(33) Zhu, Y.; Wu, Z.; Jing, M.; Hou, H.; Yang, Y.; Zhang, Y.; Yang, X.; Song, W.; Jia, X.; Ji, X. Porous $NiCo_2O_4$ Spheres Tuned Through Carbon Quantum Dots Utilised as Advanced Materials for an Asymmetric Supercapacitor. *J. Mater. Chem. A* **2015**, *3*, 866−877.
(34) Wang, B.; Williams, R. G.; Chang, Z.; Jiang, M.; Liu, J.; Lei, X.; Sun, X. Hierarchical NiAl Layered Double Hydroxide/Multiwalled Carbon Nanotube/Nickel Foam Electrodes with Excellent Pseudocapacitive Properties. *ACS Appl. Mater. Interfaces* **2014**, *6*, 16304−16311.
(35) Li, L.; Zhang, Y.; Shi, F.; Zhang, Y.; Zhang, J.; Gu, C.; Wang, X.; Tu, J. Spinel Manganese-Nickel-Cobalt Ternary Oxide Nanowire Array for High-Performance Electrochemical Capacitor Applications. *ACS Appl. Mater. Interfaces* **2014**, *6*, 18040−18047.
(36) Fan, Z.; Yan, J.; Wei, T.; Zhi, L.; Ning, G.; Li, T.; Wei, F. Asymmetric Supercapacitors Based on Graphene/MnO_2 and Activated Carbon Nanofiber Electrodes with High Power and Energy Density. *Adv. Funct. Mater.* **2011**, *21*, 2366−2375.
(37) Wu, S.; Chen, W.; Yan, L. Fabrication of a 3D MnO_2/Grapheme Hydrogel for High-Performance Asymmetric Supercapacitors. *J. Mater. Chem. A* **2014**, *2*, 2765−2772.
(38) Li, L.; Hu, A. Z.; An, N.; Yang, Y. Y.; Li, M. Z.; Wu, Y. H. Facile Synthesis of MnO_2/CNTs Composite for Supercapacitor Electrodes with Long Cycle Stability. *J. Phys. Chem. C* **2014**, *118*, 22865−22872.
(39) Chen, W.; Xia, C.; Alshareef, H. N. One-Step Electrodeposited Nickel Cobalt Sulfide Nanosheet Arrays for High-Performance Asymmetric Supercapacitors. *ACS Nano* **2014**, *8*, 9531−9541.
(40) Yu, C.; Ma, P.; Zhou, X.; Wang, A.; Qian, T.; Wu, S.; Chen, Q. All-Solid-State Flexible Supercapacitors Based on Highly Dispersed Polypyrrole Nanowire and Reduced Graphene Oxide Composites. *ACS Appl. Mater. Interfaces* **2014**, *6*, 17937−17943.
(41) Jana, M.; Saha, S.; Khanra, P.; Samanta, P.; Koo, H.; Murmu, C. N.; Kuila, N. T. Non-Covalent Functionalization of Reduced Graphene Oxide Using Sulfanilic acid Azocromotrop and Its Application as a Supercapacitor Electrode Material. *J. Mater. Chem. A* **2015**, *3*, 7323−7331.

DOI: 10.1021/acsami.5b03562
ACS Appl. Mater. Interfaces 2015, 7, 14211−14222